Regularization and analysis of GRACE mass anomaly time series by a minimization of month-to-month year-to-year double differences

Ditmar, Pavel

Publication date
2018

Document Version
Final published version

Citation (APA)
Ditmar, P. (2018). *Regularization and analysis of GRACE mass anomaly time series by a minimization of month-to-month year-to-year double differences*. Poster session presented at 9th Hotine-Marussi Symposium, Rome, Italy.

Regularization and analysis of GRACE mass anomaly time series by a minimization of month-to-month year-to-year double differences

Pavel Ditmar

Delft University of Technology
The Netherlands

Email: P.G.Ditmar@tudelft.nl

Abstract

A methodology has been developed to estimate the accuracy of GRACE monthly solutions as functions of space or time without using independent geophysical models. An application of the methodology to several commonly-used solution time-series reveals that the ITSG-Grace2016 solutions show the highest accuracy among those considered. Furthermore, it is found that the accuracy of background models exploited to produce GRACE RL05 solutions was likely insufficient to describe adequately mass re-distribution in the oceans at both short (< 1 month) and long (>1 month) time scales. Insufficiently accurate modelling of ocean signals may reduce the accuracy of mass anomaly estimates not only over oceans, but also in the coastal areas of continents.

1. Introduction

Major goal: development and application of a novel methodology to analyse the accuracy of various time-series of GRACE monthly solutions.

Basic ideas:

1) **Production of a combined regularized time-series of mass anomalies per node of a regular global grid**
2) **Regularization by a minimization of Month-to-month Year-to-year Double Differences (MYDD)**
3) **Estimation of noise variances and signal variance per grid node using the Variance Component Estimation (VCE) method (Koch & Kusche, 2002)**
4) **Computing time-series of average noise variances for pre-defined regions and globally.**

2. Methodology

2,1 Observation equations:

$$\begin{cases} \mathbf{x} = \mathbf{d_1} \\ \dots \\ \mathbf{x} = \mathbf{d_n} \\ \mathbf{Dx} = \mathbf{0}, \end{cases}$$

where $\mathbf{d_1}$,... $\mathbf{d_n}$ are the original time-series; and $\mathbf{x}$ is the regularized time-series. The last equation defines the set of "pseudo-observations" which are responsible for the regularization; $\mathbf{D}$ is the operator to compute MYDDs, see below.

2,2 Regularization by minimization of month-to-month year-to-year double differences

Month-to-month year-to-year double differences (MYDDs):

$\mathbf{Dx}$ is a finite-difference analog of the expression $\dot{\xi}_{k+1}(t) - \dot{\xi}_k(t)$, where $\xi_k(t)$ is a time-series of mass anomalies in the k-th year,

$$\dot{\xi}_k(t) = \frac{\partial \xi_k(t)}{\partial t},$$

and t is time in years.

Regularization function:

$$\Omega[\mathbf{x}] = \mathbf{x}^T \mathbf{D}^T \mathbf{D}\mathbf{x} = \sum_{k=1}^{K-1} \int_0^1 \left(\dot{\xi}_{k+1}(t) - \dot{\xi}_k(t)\right)^2 dt,$$

where K is number of years.

Penalty function:

$$\Phi[\mathbf{x}] = \sum_{j=1}^{n} \left[\frac{1}{\sigma_j^2} (\mathbf{d_j} - \mathbf{x})^T (\mathbf{d_j} - \mathbf{x})\right] + \frac{1}{\sigma_{\text{sig}}^2} \Omega[x],$$

where σ_j^2 is the noise variance of the j-th time-series, and σ_{sig}^2 is the signal variance.

2,3 Physical interpretation of the adopted regularization

According to the mass balance equation, the rate of mass change in a particular river basin or ice drainage system is equal to the difference between mass gain (i.e., precipitation) and mass loss (e.g., due to evaporation, transpiration, sublimation, water run-off, or ice discharge). Thus, the adopted regularization functional does not penalize the mass anomaly signals that reflect stationary climatological conditions (i.e., when the mass gains and mass losses per calendar month do not change from year to year). Further analysis of this regularization condition can be found in (Ditmar et al, 2018)

2,4 Estimation of signal variance

Regularized time-series:

$$\hat{\mathbf{x}} = \mathbf{N}^{-1} \sum_{j=1}^{n} \left[\frac{1}{\sigma_j^2} \mathbf{d_j}\right],$$

where $\mathbf{N}$ is the normal matrix:

$$\mathbf{N} = \sum_{j=1}^{n} \left[\frac{1}{\sigma_j^2} \mathbf{I}\right] + \frac{1}{\sigma_{\text{sig}}^2} \mathbf{D}^T \mathbf{D}.$$

Estimated signal variance:

$$\hat{\sigma}_{\text{sig}}^2 = \frac{1}{m_x - \tau_x} \mathbf{x}^T \mathbf{D}^T \mathbf{D}\mathbf{x},$$

where m_x is the number of pseudo-observations (MYDDs) and

$$\tau_x = \text{trace}\left[\frac{1}{\sigma_{\text{sig}}^2} \mathbf{D}^T \mathbf{D} \mathbf{N}^{-1}\right].$$

2,5 Estimation of noise variances

Estimated noise variance of the j-th time-series:

$$\hat{\sigma}_j^2 = \frac{1}{m_j} \mathbf{e_j}^T \mathbf{e_j},$$

where m_j is the number of observations in the j-th time-series and $\mathbf{e_j}$ are the post-fit residuals scaled in such a way that the averaging of their squares results in an unbiased estimate of the noise variance:

$$\mathbf{e_j} = \sqrt{\frac{m_j}{m_j - \tau_j}} (\mathbf{d_j} - \mathbf{x})$$

with

$$\tau_j = \text{trace}\left[\frac{1}{\sigma_j^2} \mathbf{N}^{-1}\right].$$

The computations presented in Sect. 2.4 and 2.5 are performed iteratively, starting from certain initial values of σ_{sig}^2 and σ_j^2 $(j = 1, \dots n)$.

2,6 Estimation of the spatially-averaged noise variance time series

$$\hat{\sigma}_j^2(t) = \frac{1}{S_\Omega} \iint_\Omega \left(\mathbf{e_j}(\theta, \lambda, t)\right)^T \left(\mathbf{e_j}(\theta, \lambda, t)\right) d\Omega,$$

where (θ, λ) are the geographical coordinates of a current point, Ω is the study region, and S_Ω is the area of the study region.

3.Results

3.1 Post-processing of GRACE monthly solutions

- **Considered solutions: GFZ RL05, CSR RL05, and ITSG-Grace2016**
- **Time interval: Apr. 2002 – Dec. 2013**
- **Maximum degree (L_{max}): 60**
- **Degree-1 and C_{20} coefficients: from (Sun et al, 2017)**
- **Filtering: Gaussian filter of 400-km half-width**
- **Mass anomalies are computed at the reference ellipsoid (Ditmar, 2018)**

3.2 Time-series of globally averaged accuracy of mass anomalies

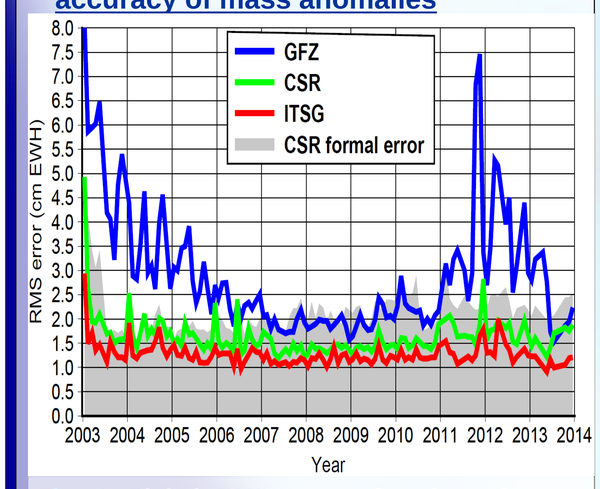

Fig. 1 Global RMS error of estimated mass anomalies as a function of time. ITSG solutions show the lowest noise level (in average, 1.2 cm EWH) followed by CSR solutions (1.7 cm) and GFZ solutions (3.2 cm). All the solutions show increased noise levels in 2003 and in 2011-2012. A reduction of noise level in 2013 is observed, which is likely due to rapid lowering the GRACE orbits in the last years of the satellite mission.

3.3 Accuracy of mass anomaly estimates as a function of spatial coordinates

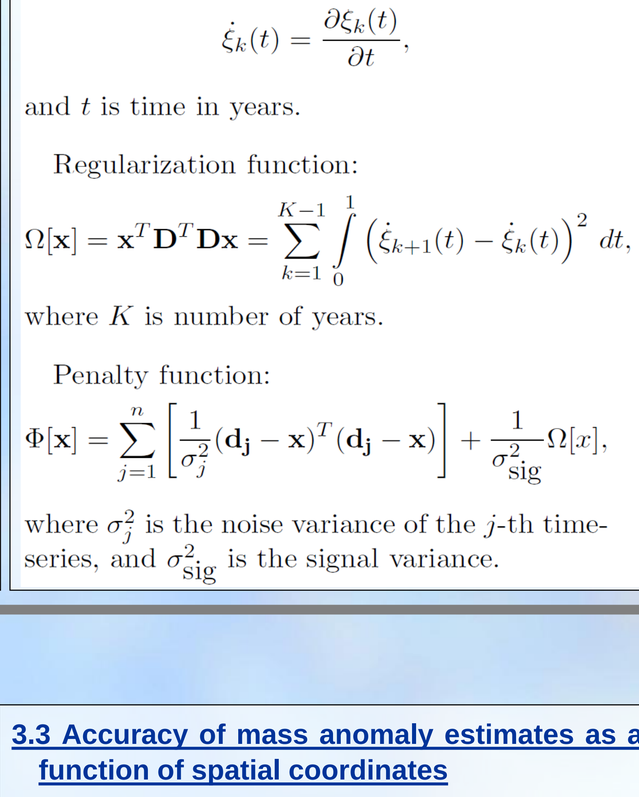

Fig. 2 RMS errors of mass anomalies derived from ITSG (top) and CSR (bottom) monthly solutions, as functions of spatial coordinates (cm EWH). The 400-km Gaussian is additionally applied to improve the visibility of the obtained maps. The accuracy is highest in the polar areas and reduces towards the equator. Remarkably, the accuracy of estimates over Eurasia and North America is higher than over the ocean locations at the same latitudes. This is an evidence that the accuracy of background models exploited to produce CSR RL05, ITSG-Grace2016 was likely insufficient to describe adequately the mass re-distribution in the oceans at the sub-monthly time scale. This finding is further confirmed by Fig. 3 below.

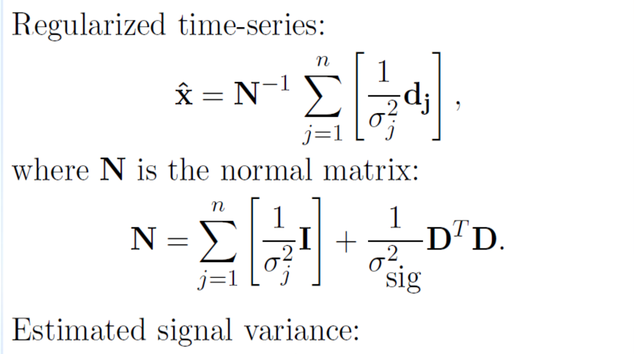

Fig. 3 RMS errors of mass anomalies derived from ITSG and CSR solutions, as well as formal errors in mass anomalies derived from CSR full error variance-covariance matrices (cm EWH). The errors are averaged in time and space. Six latitude bands are considered (three bands per hemisphere): two polar bands ($\varphi > 60^o$), two mid-latitude bands ($30^o > \varphi > 60^o$), and two tropical bands ($\varphi < 30^o$), as well as the entire globe. The ITSG solutions show a superior performance in all latitude bands. Remarkably, the mid-latitude band in the southern hemisphere shows a significantly higher noise level than a similar band in the northern hemisphere. A comparison of the corresponding formal errors shows that this effect cannot be explained by a geometry of satellite orbits. Therefore, an increased noise level over oceans remains the most likely explanation. This conclusion is further confirmed by a zoom-in on Europe (Fig.4).

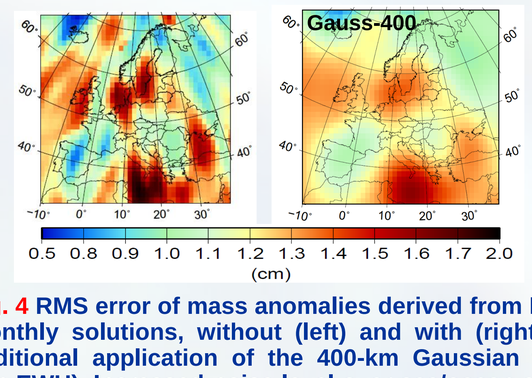

Fig. 4 RMS error of mass anomalies derived from ITSG monthly solutions, without (left) and with (right) an additional application of the 400-km Gaussian filter (cm EWH). Increased noise level over sea/ocean areas is clearly visible. Remarkably, increased noise levels are observed also in the coastal areas of the European continent, including the Netherlands.

3,4 RMS signal in mass anomaly estimates (in terms of MYDD)

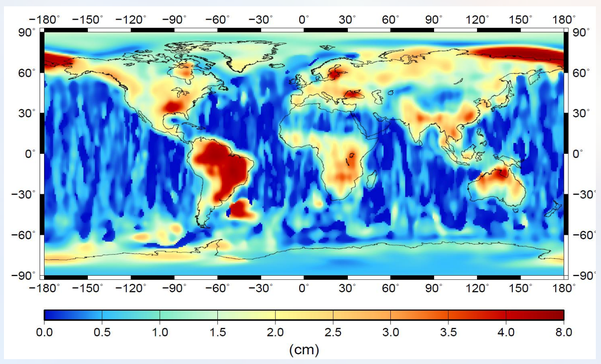

Fig. 5 RMS signal in mass anomaly estimates extracted from a combination of the three considered GRACE monthly solution time-series (in terms of MYDD, cm EWH). A sufficiently strong signal is observed not only over many continental areas (as expected), but also over the Russian coasts of the Arctic Ocean, some inner seas and bays (Baltic Sea, Black Sea, Hudson Bay), the Argentine Basin in the South Atlantic, the Gulf of Carpentaria, and some other ocean areas. This is an evidence that the exploited background models could not clean GRACE data from all the ocean signals at the monthly and longer time scales.

4.Conclusions

- **The developed methodology allows the accuracy of GRACE monthly solutions to be estimated as functions of space or time without using independent geophysical models**
- **ITSG-Grace2016 solutions show the highest accuracy among those considered**
- **The solutions show a higher accuracy of mass anomaly estimates over Eurasia and North America, as compared to the ocean locations at the same latitudes**
- **Accuracy of background models exploited to produce GRACE RL05 solutions was likely insufficient to describe adequately mass re-distribution in the oceans at both short (< 1 month) and long (>1 month) time scale.**
- **Insufficiently accurate modelling of ocean signals my reduce the accuracy of mass anomaly estimates not only over oceans, but also in the coastal areas of continents.**

References:

Ditmar, P., 2018. Conversion of time-varying Stokes coefficients into mass anomalies at the Earth's surface considering the Earth's oblateness, Journal of Geodesy, doi: 10.1007/s00190-018-1128-0.

Ditmar, P., Ran, N.T.J., and Klees, R., 2018. Estimation and reduction of random noise in mass anomaly time-series from satellite gravity data by minimization of month-to-month year-to-year double differences, Journal of Geodynamics, 119, 9–22.

Koch, K.R. and Kusche, J., 2002. Regularization of geopotential determination from satellite data by variance components, Journal of Geodesy, 76, 259–268.

Sun, Y., Ditmar, P., and Riva, R., 2017. Statistically optimal estimation of degree-1 and C_{20} coefficients based on GRACE data and an ocean bottom pressure model, Geophysical Journal International, 210(3), 1305–132.

TU Delft

Delft University of Technology